REVISTA INTERDISCIPLINAR DE PESQUISA EM ENGENHARIA

CILAMCE 2016

XXXVII IBERIAN LATIN AMERICAN CONGRESS ON COMPUTATIONAL METHODS IN ENGINEERING
BRASÍLIA - DF - BRAZIL

ON THE USE OF A CONTINUOUS STRONG–FORM RESIDUUM FIELD FOR ERROR ESTIMATION IN SMOOTH *GFEM* APPROXIMATIONS

Diego Amadeu F. Torres

diego.amadeu@gmail.com

Department of Mechanical Engineering, Federal University of Technology of Paraná - UTFPR

Avenida dos Pioneiros 3131, Jardim Morumbi, Londrina, 86036–370, Paraná, Brazil

Clovis Sperb de Barcellos

clovis.barcellos@gmail.com

Graduate Program of Mechanical Engineering, Federal University of Santa Catarina - UFSC

Trindade Campus, Florianópolis, 88040–900, Santa Catarina, Brazil

Felício Bruzzi Barros

felicio@dees.ufmg.br

Department of Structural Engineering, Federal University of Minas Gerais - UFMG

Avenida Antônio Carlos 6627, Pampulha, Belo–Horizonte, 31270–901, Minas Gerais, Brazil

Abstract. *This investigation proposes the use of continuous strong–form residuum fields, obtained through smooth Generalized Finite Element Method (GFEM) , for error estimation in terms of the energy norm. Aspects on the construction of C^k–GFEM–based approximation functions (Duarte, Kim & Quaresma, 2006), using domain triangulation, are addressed. It is shown how the smoothness may be exploited in implicit residual algorithms for error estimation since the approximated C^k–GFEM stress field can be directly continuously differentiated, to verify the equilibrium equations in strong form, locally, and then leading to a continuous*

residuum field. The subdomain strategy (Barros et al., 2013; Parés, Díez & Huerta, 2006) for implicit error estimation is employed, in such a way the local error problems are defined on the clouds, the patch of elements around the node, through the weighting provided by the Partition of Unity (PoU) functions. Its implementation fits very well into GFEM routines because such strategy is naturally tailored to the nodal enrichment procedure of the method (Barros, Barcellos & Duarte, 2007), producing nodal error indicators. Two types of weighting for the variational residuum functional (Prudhomme et al., 2004; Strouboulis et al., 2006) are tested in order to verify the performance for the effectivity of the nodal indicators and the global estimators. Numerical examples show that both the indicator and the estimator may be effective for two-dimensional linear elastic problems even in the presence of singularities.

Keywords: *subdomain error estimators, implicit residual methods, C^k–GFEM, smoothness, strong-form residuum field*

1 INTRODUCTION

Even though element–based implicit residual methods with Neumann boundary conditions lead to good estimatives of the error in energy norm they are generally expensive since such methods take into account the lack of smoothness of the approximate solution in the measure of the error. Because of this, the post–processing of numerical fluxes to minimize their jumps over the edges and the use of equilibration processes for building boundary data for Neumann local problems compatible with the interior residuals are demanded. In addition, such equilibration is generally carried out variationally using standard methods. The idea remounts to Ladevèze & Leguillon (1983) where the fluxes are built from dual solutions in local problems. Some equilibrating conditions with the derivation of their local systems of linear equations for approximated solutions are presented in Ainsworth & Oden (2000), whilst in Anuvriev, Korneev & Kostylev (2007) the use of exact equilibrated fields from the differential governing equations for the purpose of error estimation is advocated.

Differently, cloud–based implicit residual error estimators, also referred to as subdomain–based error estimators (Morin, Nochetto & Siebert, 2003), employ the concept of Partition of Unity (PoU) for weighting the residual functional or the bilinear form in terms of the error, or both, in the variational representation of the error. Some approaches were proposed by Prudhomme et al. (2004), Pares, Diez, & Huerta (2006) and Strouboulis et al. (2006). In this way, the local error problems are defined on the clouds, the patch of elements around the node. The weighting using such PoU, which naturally vanishes on the cloud boundaries, leads to null Neumann boundary datas since the presence of the PoU in the residuum expression nullifies any integration along the boundary of inner clouds. Moreover, the traction jumps across element faces inside the cloud are implicitly taken into account and the error is searched in the so–called broken spaces. Its implementation fits very well into GFEM routines (Strouboulis, Babuška & Copps, 2000; Strouboulis, Copps & Babuška, 2001; Strouboulis, Zhang & Babuška, 2003; Strouboulis et al., 2006) because such strategy is naturally tailored to the nodal enrichment procedure of GFEM (Barros, Barcellos & Duarte, 2007; Barros et al., 2013), then producing nodal error indicators.

In this scenario, from the observation that the flux of the exact solution is, in general, continuous even though finite elements are not able to provide this, interesting advantages may be

reached employing ansatz spaces with some regularity. The arbitrarily continuous approximation functions that can be built through the so–called C^k–GFEM framework (Duarte, Kim & Quaresma, 2006) from smooth weighting functions associated to free-form polygonal clouds are convenient for looking forward alternative approaches. Cloud edge functions with the desired continuity are combined to generate the weighting functions and these are used to define the PoU. The resulting PoU can be extrinsically enriched to build approximation spaces for solving variational Boundary Value Problems (*BVP*), and such approach may be considered a special instance of the *hp*–clouds method (Duarte & Oden ,1996; Oden, Duarte & Zienkiewicz, 1998).

The purpose of this work is to investigate the advantages of smooth PoU for error estimation in energy norm. Aspects as the construction of C^k–GFEM based approximation functions using domain triangulation are addressed and it is shown how the continuity may be exploited in implicit residual algorithms (Ainsworth & Oden, 2000) for error estimation since there are no stress jumps at element boundaries and, in addition, the approximated stress field can be directly differentiated in order to compute the equilibrium equations in strong–form and, thus, obtaining a continuous residuum fields. As a consequence, such residuum fields may be projected over a set of higher order functions, in other words, a conveniently defined reference space for error estimate purposes, resulting in the loading term for the variational error problem posed on the clouds. Two types of weighting the local problems are tested to verify the performance for the effectivity index provided by the nodal indicators and by the global estimator.

2 MODEL PROBLEM

Let's consider the static linear elasticity problem for a elastic body $\Omega \in \mathbb{R}^2$, viewed as a planar-bounded Lipschitz domain with polygonal boundary $\partial\Omega$. The *strong form* of a *BVP*, using matrix notation, states: *seek a displacement field* $\boldsymbol{u}(\boldsymbol{x}) = \{u_x, u_y\}^T \in \mathcal{H}^1\left(\Omega;\mathbb{R}^2\right)$ (the superscript T indicates transpose) *that satisfy the equilibrium equations*

$$\boldsymbol{L}^T\boldsymbol{\sigma}(\boldsymbol{u}) + \boldsymbol{b} = \boldsymbol{0} \text{ in } \Omega \tag{1}$$

and the boundary conditions, $\boldsymbol{u} = \overline{\boldsymbol{u}}$ on Γ_D *and* $\boldsymbol{t}(\boldsymbol{u}) = \boldsymbol{n}\boldsymbol{\sigma} = \bar{\boldsymbol{t}}$ on Γ_N. Here, $\mathcal{H}\left(\Omega;\mathbb{R}^2\right)$ is the Hilbert space of degree one, the space of square-integrable functions with square-integrable weak derivatives (Oden & Reddy, 1976; Kreyszig, 1989).

The equilibrium equations, Eq. (1), establishes the local (pointwise, for all position $\boldsymbol{x} = \{x,y\}^T \in \Omega$) balance of forces per unit volume (Boresi, Chong & Lee, 2011), where the stresses $\boldsymbol{\sigma} = \{\sigma_x, \sigma_y, \tau_{xy}\}^T$ (each component also being function of the independent variable $\boldsymbol{x}$, which will be omitted thereafter to keep the notation simpler) are subjected to a differential operator $\boldsymbol{L}$ and $\boldsymbol{b} = \{b_x, b_y\}^T \in \mathcal{L}^2\left(\Omega;\mathbb{R}^2\right)$ is the vector of components of applied volume forces, with $\mathcal{L}^2(\Omega;\mathbb{R}^2)$ being the space of Lebesgue measurable functions with integrable squares on Ω. The vector $\bar{\boldsymbol{t}} = \{t_x, t_y\}^T \in \mathcal{L}^2\left(\Omega;\mathbb{R}^2\right)$ contains the components of external applied forces per unit of surface area on some (relatively open) part Γ_N of the boundary $\partial\Omega$ with exterior unit normal vector $\boldsymbol{n} \in \mathcal{L}^\infty\left(\partial\Omega;\mathbb{R}^{2\times 3}\right)$. Additionally, the body is supported on the remaining closed part $\Gamma_D := \partial\Omega \setminus \Gamma_N$ where the displacement field is prescribed by the Dirichlet data $\overline{\boldsymbol{u}}$. Finally, the operators $\boldsymbol{L}$ and $\boldsymbol{n}$ are defined as

$$\boldsymbol{L} = \begin{bmatrix} \frac{\partial}{\partial x} & 0 \\ 0 & \frac{\partial}{\partial y} \\ \frac{\partial}{\partial y} & \frac{\partial}{\partial x} \end{bmatrix} \quad \text{and} \quad \boldsymbol{n} = \begin{bmatrix} n_x & 0 & n_y \\ 0 & n_y & n_x \end{bmatrix}. \tag{2}$$

In linear elasticity, the stresses are related to the strains through the linear elastic constitutive relation $\boldsymbol{\sigma} = \boldsymbol{C}\boldsymbol{\varepsilon}$, with $\boldsymbol{C} \in \mathcal{L}^{\infty}\left(\Omega;\mathbb{R}^{3\times 3}\right)$ being a constitutive matrix, and the strains $\boldsymbol{\varepsilon} = \{\varepsilon_x, \varepsilon_y, \gamma_{xy}\}^T$, in turn, are related to the displacements by $\boldsymbol{\varepsilon} = \boldsymbol{L}\boldsymbol{u}$, the linear strain-displacement relationship.

On the other hand, the corresponding continuous variational form of this problem can be stated as: *find* $\boldsymbol{u} \in \mathcal{U}$, *such that*

$$\mathscr{B}(\boldsymbol{u}, \boldsymbol{v}) = \mathscr{L}(\boldsymbol{v}), \quad \forall\, \boldsymbol{v} \in \mathcal{V} \tag{3}$$

where an equilibrium condition is now established in the global sense and no longer in the local sense (Brebbia, Telles & Wrobel, 1984). The so-called *weak solution* (Babuška, Whiteman & Strouboulis, 2011) is sought in the set of kinematically admissible functions, defined as

$$\mathcal{U} := \left\{\mathcal{H}^1\left(\Omega;\mathbb{R}^2\right) : \boldsymbol{u} = \overline{\boldsymbol{u}} \text{ on } \Gamma_D\right\} \tag{4}$$

and the kinematically admissible variations lie in the restriction of $\mathcal{H}^1\left(\Omega;\mathbb{R}^2\right)$ with homogeneous Dirichlet boundary values, such that

$$\mathcal{V} := \mathcal{H}^1_D\left(\Omega;\mathbb{R}^2\right) := \left\{\boldsymbol{v} \in \mathcal{H}^1\left(\Omega;\mathbb{R}^2\right) : \boldsymbol{v} = \boldsymbol{0} \text{ on } \Gamma_D\right\}. \tag{5}$$

The bilinear form $\mathscr{B}(\boldsymbol{u}, \boldsymbol{v})$ in (3), physically meaning the virtual work of the internal stresses associated with the strains $\boldsymbol{\epsilon}$ related to the virtual displacement $\boldsymbol{v}$, is a functional on $\mathcal{H}^1 \times \mathcal{H}^1 \to \mathbb{R}$ defined as

$$\mathscr{B}(\boldsymbol{u}, \boldsymbol{v}) := \int\int_{\Omega} \boldsymbol{\varepsilon}^T(\boldsymbol{v})\, \boldsymbol{\sigma}(\boldsymbol{u})\, l_z\, dx\, dy \tag{6}$$

and $\mathscr{L}(\boldsymbol{v})$ is a linear functional $\mathcal{H}^1 \to \mathbb{R}$, which represents the virtual work resulting from the external applied forces, defined as

$$\mathscr{L}(\boldsymbol{v}) := \int\int_{\Omega} \boldsymbol{v}^T\, \boldsymbol{b}\, l_z\, dx\, dy + \int_{\Gamma_N} \boldsymbol{v}^T\, \bar{\boldsymbol{t}}\, l_z\, ds \tag{7}$$

where l_z is the thickness of the body, assumed here as constant by simplification.

The bilinear form in Eq. (6) induces the definition of the energy norm as

$$\|\boldsymbol{u}\|_E := \sqrt{\mathscr{B}(\boldsymbol{u},\boldsymbol{u})} \tag{8}$$

because its physical meaning is related to the energy of the system. A complete explanation about variational formulation for the finite element method can be found in Babuška, Whiteman & Strouboulis (2011).

In the next section, a brief explanation on the chosen discretization method is presented. The aim of such choice is to obtain approximations to the problem in Eq. (3) with higher regularity, featuring continuous stress fields. As a consequence, a new approach will be proposed for a posteriori error estimation.

3 APPROXIMATION FUNCTIONS CONSTRUCTION

In order to define the discretized version of the *BVP* under consideration, let us consider a conventional finite element triangulation, $\{\mathcal{K}_e\}_{e=1}^{NE}$ (*NE* being the number of elements in $\mathcal{K}_e$), defined by N nodes with coordinates $\{\boldsymbol{x}_\alpha\}_{\alpha=1}^{N}$, in an open-bounded polygonal domain $\Omega \subset \mathbb{R}^2$. The interior of the union of all finite elements sharing each of these nodes is denoted as a *cloud*, $\omega_\alpha, \alpha = 1,...,N$, as usually cited in the generalized finite element method (GFEM) literature (Duarte, Babuška & Oden, 2000; Strouboulis, Babuška & Copps, 2000; Fries & Belytschko, 2010).

In this work, it is proposed to use approximation functions with arbitrary continuity, k, aiming to approximate continuous stress fields and, as a consequence, to obtain continuous strong-form residuum fields. Thus, the C^k-GFEM (Duarte, Kim & Quaresma, 2006) is employed. Such special instance of the GFEM is a methodology designed to build mesh-based approximations with higher regularity, in which the PoU functions are the Shepard ones (Shepard, 1968), considering smooth weighting functions defined on the clouds. The weighting functions, in turn, are computed from *cloud edge functions*, which are defined in global coordinates though a procedure that is completely free of geometric restrictions for the elements and for the nodal patches (Barcellos, Mendonça & Duarte, 2009; Mendonça, Barcellos & Torres, 2011; Mendonça, Barcellos & Torres, 2013; Torres, Barcellos & Mendonça, 2015; Freitas et al., 2015).

The C^k-GFEM allows to recover the smoothness typical of moving-least squares-based meshfree methods (Liu, 2003) even considering element meshes. Additionally, the extrinsic procedure of enrichment, as proposed in the *hp*-cloud method (Duarte, 1996), favors the adaptive algebraic enrichment, either using polynomial p-enrichment functions or tailored functions for specific problems, as in crack modeling common in XFEM works (Belytschko & Black, 1999; Stazi et al., 2003), grain boundary effects in polycrystal materials (Simone, Duarte & Van der Giessen, 2006), mesoscale modeling of dislocations (Belytschko & Gracie, 2007), to cite a few examples.

Let $\Im_N$ be an open covering of the domain Ω built by the set of N clouds ω_α, that is, the closure $\overline{\Omega}$ of the domain is contained in the union of the cloud closures $\overline{\omega}_\alpha$

$$\overline{\Omega} \subset \cup_{\alpha=1}^{N} \overline{\omega}_\alpha \ . \tag{9}$$

In addition, consider a set of functions $S_N = \{\varphi_\alpha(\boldsymbol{x})\}_{\alpha=1}^N$, each having the corresponding cloud ω_α as its compact support. If this set has the property that each one of these functions is such that $\varphi_\alpha(\boldsymbol{x}) \in C_0^k(\omega_\alpha), k \geqslant 0$ and $\sum_{i=1}^N \varphi_\alpha(\boldsymbol{x}) = 1$, $\forall\ \boldsymbol{x}\in\Omega$, and every compact subset of Ω intersects only a finite number of supports, then the set $\{\varphi_\alpha(\boldsymbol{x})\}$, $\alpha = 1,...,N$ is said to be a Partition of Unity, PoU, subordinated to the covering $\Im_N$ (Oden & Reddy, 1976). The first requirement indicates that a function φ_α is non-zero only over its respective cloud ω_α and is, at least, k times continuously differentiable.

There are several kinds of PoU used in computational mechanics and the Lagrangian FEM shape functions are just one type, which is in $C_0^0(\omega_\alpha)$. Additional examples can be found in several meshless methods, such as the *hp*-cloud method. Another example, the Shepard scheme, makes use of *weighting functions,* $\mathcal{W}_\alpha : \mathbb{R}^2 \to \mathbb{R}$, with the cloud ω_α as their compact support[1], such that $\mathcal{W}_\alpha$ belongs to the space $C_0^k(\omega_\alpha)$. The Shepard PoU functions subordinated to the covering $\Im_N$ are defined as

$$\varphi_\alpha(\boldsymbol{x}) = \frac{\mathcal{W}_\alpha(\boldsymbol{x})}{\sum_{\beta(\boldsymbol{x})} \mathcal{W}_\beta(\boldsymbol{x})},\ \ \beta(\boldsymbol{x}) \in \left\{\gamma \mid \mathcal{W}_\gamma(\boldsymbol{x}) \neq 0\right\}\ . \tag{10}$$

Therefore, the regularity of these PoU functions relies only on the regularity of the weighting functions. The weighting function, in turn, can be defined as the product of all cloud edge functions $\varepsilon_{\alpha,j}$ as

$$\mathcal{W}_\alpha(\boldsymbol{x}) := \prod_{j=1}^{M_\alpha} \varepsilon_{\alpha,j}\left(\xi_j\right) \tag{11}$$

in case of a convex cloud ω_α, where M_α is the number of cloud edge functions associated with the cloud.

Finally, the only component that needs to be defined is the *cloud edge function*, $\varepsilon_{\alpha,j}$. A cloud edge function is a function which vanishes, together with its k derivatives, as this edge is approached and is strictly positive in the interior of the cloud. In Eq. (11) the dependency on the parametric coordinate $\left(\xi_j\right)$ is made evident. Such a parametric coordinate is defined inside the cloud for each edge, being normal to it and growing towards the cloud node. A complete description on the procedure may be found in Torres (2012) and Barcellos, Mendonça & Duarte (2009).

Many functions meet the pointed requirements for a cloud edge function and in Barcellos, Mendonça & Duarte (2009) polynomials and exponential functions were subjected to numerical investigations. Herein, exponential edge functions are used, considering $\gamma = 0.3$ and $\beta = 0.6$ (Barcellos, Mendonça & Duarte, 2009), which guarantee $C^\infty(\Omega)$ on meshes with only convex clouds. On the contrary, if non-convex clouds are identified along the mesh, it is necessary to replace the edge functions of a pair of non-convex edges of a cloud with a single new edge function obtained through a boolean product (Rvachev & Sheiko, 1995), before to perform the weighting functions computation, as proposed by Duarte, Kim & Quaresma (2006).

[1]The GFEM scheme uses element meshes to define the clouds aiming to reduce the computational effort and to make the implementation simpler.

As commented by Mendonça, Barcellos & Torres (2011), it should be noted that the lower-regularity PoU of the standard GFEM (like lagrangian shape functions) is able to generate a complete polynomial of degree one, over the domain. Differently, the smooth PoU as described in this section is only capable of guaranteedly reproducing a unitary constant functions, even though it can generate something else but not polynomial. This low reproducibility makes necessary the application of polynomial enrichments to assure convergence.

Basically, GFEM proposes that a local approximation subspace $\mathcal{X}_\alpha(\omega_\alpha)$ may be chosen for each cloud ω_α in such a way that one or some enrichment functions $\mathcal{L}_{\alpha i} \in \mathcal{X}_\alpha(\omega_\alpha)$ can closely approximate $\boldsymbol{u}|_{\omega_\alpha}$ over the cloud ω_α, without compromising the conforming requirement since each $\mathcal{L}_{\alpha i}$ is multiplied by the PoU of the node α.

Thus, the PoU functions can be enriched by multiplying any of them by a set of enrichment functions, $\{\mathcal{L}_{\alpha i}\}_{i\in\mathcal{I}(\alpha)}$, where $\mathcal{I}(\alpha)$, $\alpha = 1,...,N$, is an index set of known functions, for instance, polynomials, generalized harmonic functions, boundary layer functions, particular solutions to similar problems, singular solutions to the specific problem under consideration, and anisotropic functions. Therefore, the local approximation subspaces, denoted as $\chi_\alpha(\omega_\alpha) = span\{\mathcal{L}_{\alpha i}\}_{i\in\mathcal{I}(\alpha)}$, may also be enriched according to an adaptive method.

For instance, a set of polynomial enrichment functions $\mathcal{L}^p_{\alpha i}$ of a node α which involves nine polynomial functions such as

$$\mathcal{L}^p_{\alpha i}(x,y) = \left\{\bar{x},\ \bar{y},\ \bar{x}^2,\ \bar{x}\,\bar{y},\ \bar{y}^2,\ \bar{x}^3,\ \bar{x}^2\,\bar{y},\ \bar{x}\,\bar{y}^2,\ \bar{y}^3\right\},\ \ i = 9 \text{ and } p = 3 \tag{12}$$

can span the set of polynomials of degree $p \leq 3$. In this work, a scaling is performed by a characteristic length h_{x_α} of the cloud, which can be taken as the largest distance parallel to the x-axis from the node $\boldsymbol{x}_\alpha$ to each of their cloud edges, such that the intrinsic coordinate $\bar{x}$, for example, is defined as $\bar{x} := (x - x_\alpha)/h_{x_\alpha}$. A similar treatment is employed for the $\bar{y}$ monomials. This strategy has been used in Torres, Mendonça & Barcellos (2011) and Torres, Barcellos & Mendonça (2015).

Therefore, the cloud functions family $\mathcal{F}^p_N$ is composed by the union between the PoU and enriched functions as

$$\mathcal{F}^p_N = \left\{ \{\varphi_\alpha(\boldsymbol{x})\}_{\alpha=1}^N \bigcup \left\{ \varphi_\alpha(\boldsymbol{x})\mathcal{L}^p_{\alpha i}(\boldsymbol{x}) \right\}_{\alpha=1}^N | i \in \mathcal{I}(\alpha) \right\} \tag{13}$$

where $\varphi_\alpha(\boldsymbol{x})$ are PoU functions and $\mathcal{L}^p_{\alpha i}(\boldsymbol{x})$ are the enrichment functions, both related to the node α, and $\mathcal{I}$ is an index set which refers to the enrichment functions associated with each node.

This cloud family is used to build the Galerkin approximation, e.g., for the x-component of displacement u_x, as following

$$u_{x_p}(\boldsymbol{x}) = \sum_{\alpha=1}^{N} \varphi_\alpha(\boldsymbol{x}) \left\{ u_\alpha + \sum_{i=1}^{q_\alpha} \mathcal{L}^p_{\alpha i}(\boldsymbol{x}) b_{\alpha i} \right\} = \boldsymbol{\Phi}(\boldsymbol{x})\boldsymbol{U} \tag{14}$$

where u_α and $b_{\alpha i}$ are the nodal parameters associated with the PoU $\varphi_\alpha(\mathbf{x})$, and to the enriched functions $\varphi_\alpha(\mathbf{x})\mathcal{L}^p_{\alpha i}(\mathbf{x})$, respectively, with q_α being the number of polynomial enrichment functions of each node. In addition, for the matrix notation, $\boldsymbol{U}$ is an array of nodal coefficients and $\boldsymbol{\Phi}(\boldsymbol{x})$ is an array formed by the basis functions.

Clearly, the approximation $\boldsymbol{u}_p(\boldsymbol{x}) = \{u_{x_p}, u_{y_p}\}^T$ of the solution $\boldsymbol{u}$ of Eq. (3) is an entity of a subspace $\mathcal{U}_p \in \mathcal{U}$ (see Eq. (4)) spanned by a set of kinematically admissible GFEM approximation functions. Similarly, the subspace $\mathcal{V}_p$ is defined for composing the discretized variational problem, corresponding to Eq. (3), that is: *find* $\boldsymbol{u}_p \in \mathcal{U}_p(\Omega)$ *such that*

$$\mathscr{B}(\boldsymbol{u}_p, \boldsymbol{v}_p) = \mathscr{L}(\boldsymbol{v}_p), \ \forall\, \boldsymbol{v}_p \ \in \ \mathcal{V}_p \ . \tag{15}$$

Remark 1. When the PoU is built from polynomial finite element shape functions, as in conventional GFEM, the system of equations resulting from Eq. (15) using Eq. (14) is linearly dependent (Duarte, Babuška & Oden, 2000). In the present case, where the PoU is built as quotients of exponential functions, the resulting global stiffness matrix is positive definite if the boundary conditions imposed are sufficient to prevent rigid body motions.

Remark 2. It should be observed that the usual structure of the standard displacement-based FEM is preserved in the present formulation. The entire C^k-GFEM formulation, summarized in the present section, enters into the program structure encapsulated in a single routine, which computes the set of approximate functions as in the case of the FEM functions, which is to be used normally in the computation of the element contributions.

4 Discretization error and correspondent variational equation

Let us consider the approximated solution $\boldsymbol{u}_p$ of the discretized variational problem in Eq. (15) and built following Eq. (14). Here, considering only polynomial enrichment, the index p represents the polynomial character of the resulting approximation. Consequently, the error of an solution $\boldsymbol{u}_p$ can be defined as

$$\boldsymbol{e}_p = \boldsymbol{u} - \boldsymbol{u}_p \tag{16}$$

where $\boldsymbol{u}$ refers to the exact solution of the mathematical model in Eq. (3), such as $\boldsymbol{u} \in \mathscr{U}$ of Eq. (4). Replacing $\boldsymbol{u} = \boldsymbol{e}_p + \boldsymbol{u}_p$ in Eq. (3), and considering the linearity of the functional $\mathscr{B}(\bullet,\bullet)$ in Eq. (6) it can be found

$$\mathscr{B}(\boldsymbol{e}_p + \boldsymbol{u}_p, \boldsymbol{v}) = \mathscr{L}(\boldsymbol{v}) \ \therefore \ \mathscr{B}(\boldsymbol{e}_p, \boldsymbol{v}) = \mathscr{L}(\boldsymbol{v}) - \mathscr{B}(\boldsymbol{u}_p, \boldsymbol{v}) \ \ \forall\, \boldsymbol{v} \in \mathcal{V} \ . \tag{17}$$

A global variational equation for the error can be recovered as: *find* $\boldsymbol{e}_p \ \in \mathcal{V}$ of Eq. (5) *such as*

$$\mathscr{B}(\boldsymbol{e}_p, \boldsymbol{v}) = \mathscr{R}(\boldsymbol{v}) \quad \forall\, \boldsymbol{v} \in \mathcal{V} \tag{18}$$

where the residual functional or weak form of the residuum $\mathscr{R}(\bullet)$ is defined as

$$\mathscr{R}(\boldsymbol{v}) = \mathscr{L}(\boldsymbol{v}) - \mathscr{B}(\boldsymbol{u}_p, \boldsymbol{v}) \; . \tag{19}$$

Here, without loss of generality, it is assumed that the essential boundary conditions are exactly satisfied.

According to Díez, Parés & Huerta (2004) and Parés, Díez & Huerta (2006), the problem in Eq. (18) is decomposed into local contributions formulated over subdomains which can be the clouds of the GFEM approach, in such a way that employing the PoU property, can be obtained: *find* $\boldsymbol{e}_p \in \mathcal{V}$ *such that*

$$\mathscr{B}(\boldsymbol{e}_p, \boldsymbol{v}) = \mathscr{R}(\boldsymbol{v}) = \mathscr{R}\left(\boldsymbol{v} \sum_{\alpha=1}^{N} \varphi_\alpha\right) = \sum_{\alpha=1}^{N} \mathscr{R}(\varphi_\alpha \boldsymbol{v}) \tag{20}$$

where φ_α represents any kind of partition of unity. Since that $\mathscr{R}(\varphi_\alpha \boldsymbol{v}) = 0$ when $\omega_\alpha \cap supp(\boldsymbol{v}) = \emptyset$ the residual functional can be decomposed into local contributions, defined over each cloud.

In order to establish local problems exploiting the localization of the residual functional obtained with Eq. (20), the bilinear form is generalized to accept broken functions (Parés, Díez & Huerta, 2006) that are samples of local sub-spaces $\mathcal{V}_{\omega_\alpha}$ defined as

$$\mathcal{V}(\omega_\alpha) := \mathcal{V} \cap \mathcal{H}^1\left(\Omega, \mathbb{R}^2\right) \tag{21}$$

and, therefore, $\mathcal{V}_{brok} := \oplus_{\alpha=1}^{N} \mathcal{V}(\omega_\alpha)$ is the definition of a broken space.

Any function $\boldsymbol{v} \in \mathcal{V}(\omega_\alpha)$ of Eq. (21) is defined only over a cloud ω_α but is extended to Ω by setting the values outside ω_α equal to zero. Consequently, the error function $\boldsymbol{e}_p^{\omega_\alpha}$ will be continuous over a cloud ω_α but the summation of all *cloud error functions* $\boldsymbol{e}_p^{\omega_\alpha}$ will generate discontinuities over all interelement edges of the mesh.

Using Eq. (20), therefore, the problem in Eq. (18) can be replaced by a set of local problems defined over each cloud ω_α as: *find* $\boldsymbol{e}_p^{\omega_\alpha} \in \mathcal{V}(\omega_\alpha)$ *such as*

$$\mathscr{B}_{\omega_\alpha}^{\zeta_\alpha}\left(\boldsymbol{e}_p^{\omega_\alpha}, \boldsymbol{v}^{\omega_\alpha}\right) = \mathscr{R}_{\omega_\alpha}\left(\varphi_\alpha \boldsymbol{v}^{\omega_\alpha}\right) \; \forall \; \boldsymbol{v}^{\omega^\alpha} \in \mathcal{V}(\omega_\alpha) \; . \tag{22}$$

The *l.h.s.* of Eq. (22), the weighted bilinear form, is defined as

$$\mathscr{B}_{\omega_\alpha}^{\zeta_\alpha}\left(\boldsymbol{e}_p^{\omega_\alpha}, \boldsymbol{v}_{\omega_\alpha}\right) := \int\int_{\omega_\alpha} \zeta_\alpha \; \boldsymbol{\varepsilon}^T\left(\boldsymbol{v}^{\omega_\alpha}\right) \; \boldsymbol{\sigma}\left(\boldsymbol{e}_p^{\omega_\alpha}\right) \; l_z \, dx \, dy \tag{23}$$

and the *r.h.s.* of Eq. (22), the localized residual functional, is defined as

$$\mathscr{R}_{\omega_\alpha}(\varphi_\alpha \boldsymbol{v}^{\omega_\alpha}) = \mathscr{L}_{\omega_\alpha}(\varphi_\alpha \boldsymbol{v}^{\omega_\alpha}) - \mathscr{B}_{\omega_\alpha}(\boldsymbol{u}_p, \varphi_\alpha \boldsymbol{v}^{\omega_\alpha}) \ . \tag{24}$$

The first term of the *r.h.s.* of Eq. (24) is defined as

$$\mathscr{L}_{\omega_\alpha}(\varphi_\alpha \boldsymbol{v}^{\omega_\alpha}) = \int\int_{\omega_\alpha} (\varphi_\alpha \boldsymbol{v}^{\omega_\alpha})^T \ \boldsymbol{b}\ l_z\ dx\ dy + \int_{\partial\omega_\alpha \cap \Gamma_N} (\varphi_\alpha \boldsymbol{v}^{\omega_\alpha})^T \ \bar{\boldsymbol{t}}\ l_z\ ds \tag{25}$$

whereas the second term is written as

$$\mathscr{B}_{\omega_\alpha}(\boldsymbol{u}_p, \varphi_\alpha \boldsymbol{v}^{\omega_\alpha}) = \int\int_{\omega_\alpha} \boldsymbol{\varepsilon}^T(\varphi_\alpha \boldsymbol{v}^{\omega_\alpha})\ \boldsymbol{\sigma}(\boldsymbol{u}_p)\ l_z\ dx\ dy \ . \tag{26}$$

In Eq. (23), ζ_α represents a weighting function. In the approach proposed by Prudhomme et al. (2004) it is used $\zeta_\alpha = \varphi_\alpha$, that is, the PoU function associated to the cloud ω_α. On the other hand, can be seen that $\zeta_\alpha = 1$ in the approach of Strouboulis et al. (2006). It should be noted that

$$\mathscr{B}(\bullet,\bullet) = \sum_{\alpha=1}^{N} \mathscr{B}_{\omega_\alpha}^{\zeta_\alpha}(\bullet,\bullet) \tag{27}$$

only holds if ζ_α is also a partition of unity.

Remark 3. The the main reason of this localization is to avoid integration of stresses (or fluxes) along the boundary of inner clouds in the computation of Eq. (24), leading to local problems like Eq. (22) with homogeneous Neumann boundary conditions. The presence of the function φ_α in the residual functional of Eq. (24) nullifies any integration along the boundary of inner clouds, whereas in case of clouds along the domain boundary, the integration of the second term in the *r.h.s.* of Eq. (25) is normally performed.

Remark 4. Additionally, the error in the tractions[2] along interelement edges do not appears in the problem of Eq. (22) because, as such local problems are posed on the clouds, the effect of the tractions jumps across element edges inside the cloud is implicitly taken into account, as a subdomain approach (Díez, Parés & Huerta , 2004; Prudhomme et al., 2004; Strouboulis et al., 2006; Barros, Barcellos & Duarte, 2009; Barros et al., 2013).

Since generally it is impossible to seek for an exact solution $\boldsymbol{e}_p^{\omega_\alpha}$ for the problem in Eq. (22), here the exact error is replaced by its approximation $\widetilde{\boldsymbol{e}}_p^{\omega_\alpha}$, as suggested by (Oden et al., 1989). Thus, the approximated error will be sought from the sub-space

$$\chi_{p+q}^0(\omega_\alpha) = \left\{ \boldsymbol{v}_{p+q}^{0,\omega_\alpha} \in \chi_{p+q}(\omega_\alpha)\ ;\ \Pi_p\left(\boldsymbol{v}_{p+q}^{0,\omega_\alpha}\right) = 0\ ;\ \boldsymbol{v}_{p+q}^{0,\omega_\alpha} = 0 \ \text{ on } \partial\omega_\alpha \cap \Gamma_D \right\} \tag{28}$$

[2]Even though generally there are errors on the stresses along element edges, in C^k-GFEM approximations the stress fields are naturally continuous.

where $\Pi_p : \mathcal{V}(\omega_\alpha) \rightarrow \mathcal{X}_p(\omega_\alpha)$ is the local projector operator of degree p. In this study, the higher-order polynomial spaces $\mathcal{X}_{p+q}(\omega_\alpha) = \mathcal{X}_{p+1}(\omega_\alpha) \subset \mathcal{V}(\omega_\alpha)$ and $\mathcal{X}_{p+q}(\omega_\alpha) = \mathcal{X}_{p+2}(\omega_\alpha) \subset \mathcal{V}(\omega_\alpha)$ are tested, due to the dichotomy phenomenon, as explained in Babuška & Strouboulis (2001).

Therefore, the problem for approximating the error for Eq. (22) can be stated as: *find* $\tilde{\boldsymbol{e}}_p^{\omega_\alpha} \in \boldsymbol{\chi}_{p+q}^0(\omega_\alpha)$ *such as*

$$\mathscr{B}_{\omega_\alpha}^{\zeta_\alpha}\left(\tilde{\boldsymbol{e}}_p^{\omega_\alpha}, \boldsymbol{v}_{p+q}^{0,\omega_\alpha}\right) = \mathscr{R}_{\omega_\alpha}\left(\varphi_\alpha \boldsymbol{v}_{p+q}^{0,\omega_\alpha}\right) \quad \forall\, \boldsymbol{v}_{p+q}^{0,\omega_\alpha} \in \boldsymbol{\chi}_{p+q}^0(\omega_\alpha) \tag{29}$$

where the weighted bilinear form for the error $\mathscr{B}_{\omega_\alpha}^{\zeta_\alpha}$ and the residual functional $\mathscr{R}_{\omega_\alpha}$ are similarly defined as in Eqs. (23) and (24). Nevertheless, it is proposed in this study to replace the conventional computation of Eq. (24), which is employed in Barros et al. (2013), for instance, with

$$\mathscr{R}_{\omega_\alpha}\left(\varphi_\alpha \boldsymbol{v}_{p+q}^{0,\omega_\alpha}\right) = \mathcal{R}_\Omega^{\omega_\alpha}\left(\varphi_\alpha \boldsymbol{v}_{p+q}^{0,\omega_\alpha}\right) + \mathcal{R}_{\Gamma_N}^{\omega_\alpha}\left(\varphi_\alpha \boldsymbol{v}_{p+q}^{0,\omega_\alpha}\right) . \tag{30}$$

The first term of the *r.h.s.* of Eq. (30), $\mathcal{R}_\Omega^{\omega_\alpha}$, is an weak residual along the domain and is defined as

$$\mathcal{R}_{\omega_\alpha}\left(\varphi_\alpha \boldsymbol{v}_{p+q}^{0,\omega_\alpha}\right) := \int\int_{\omega_\alpha} \left(\varphi_\alpha \boldsymbol{v}_{p+q}^{0,\omega_\alpha}\right)^T \boldsymbol{R}(\boldsymbol{u}_p)\, l_z\, dx\, dy \tag{31}$$

where $\boldsymbol{R}(\boldsymbol{u}_p) = \{R_x, R_y\}^T$ is the strong form residuum of the approximation $\boldsymbol{u}_p$ defined as

$$\boldsymbol{R}(\boldsymbol{u}_p) := \boldsymbol{L}^T \boldsymbol{\sigma}(\boldsymbol{u}_p) + \boldsymbol{b} \tag{32}$$

since the approximation $\boldsymbol{u}_p$ solution of Eq. (15) generally does not satisfy the strong-form equilibrium equations in Eq. (1).

Remark 5. Even the strong-form residuum field defined in Eq. (32) is generally not self-equilibrated on a single cloud ω_α, an equilibrating process like that of Parés, Díez & Huerta (2006) is not necessary in this approach. It should be noted the bubble characteristic of the functions in Eq. (28) used to approximate the error. Such feature comes up because the enrichment functions of Eq. (12) for each node are always null right at the node, and consequently rigid body motions are suppressed when solving the local problems for error estimation.

The second term of the *r.h.s.* of Eq. (30), $\mathcal{R}_{\Gamma_N}^{\omega_\alpha}$ in turn, is related to the residuum along the Neumann boundary, $\boldsymbol{r}(\boldsymbol{u}_p) = \{r_x, r_y\}^T$, in strong-form, which is

$$\boldsymbol{r}(\boldsymbol{u}_p) := \bar{\boldsymbol{t}} - \boldsymbol{n}\boldsymbol{\sigma}(\boldsymbol{u}_p) \tag{33}$$

following the notation of sections 2 and 3, being the operator $\boldsymbol{n}$ defined in Eq. (2). Thus, the term $\mathcal{R}_{\Gamma_N}^{\omega_\alpha}$ is defined as

$$\mathcal{R}_{\Gamma_N}^{\omega_\alpha}\left(\varphi_\alpha \boldsymbol{v}_{p+q}^{0,\omega_\alpha}\right) := \int_{\partial\omega_\alpha\cap\Gamma_N} \left(\varphi_\alpha \boldsymbol{v}_{p+q}^{0,\omega_\alpha}\right)^T \boldsymbol{r}(\boldsymbol{u}_p)\, l_z\, ds\,. \tag{34}$$

Equation (30) consists of an inner product of the continuous strong-form residuum field expressed by Eq. (32), jointly with the residuum on the Neumann boundary as Eq. (33), with the higher order functions of an appropriate sub-space in Eq. (28) from which the error function is sought. This is the key contribution of this work and it allows to look for estimates based on the strong-form residuum field, which may be directly computed in case of smooth GFEM approximations, without any type of post-processing heuristics due to stress discontinuities common in FEM solutions.

Moreover, it should be noted that second order derivatives of the approximation $\boldsymbol{u}_p$ appear in Eq. (31) whereas Eq. (26) only involves first order derivatives of $\boldsymbol{u}_p$. Then, it is intended to compare the integration cost of these two approaches. Additionally, some improvement in the estimates can manifest, and an issue raises: *Would second order derivatives of a solution $\boldsymbol{u}_p$ of degree p contain more information than first order derivatives of functions $\boldsymbol{v}^{\omega_\alpha}$, of degree higher than p, in* (26) ?

Then, assuming that the problem data are such that $\tilde{\boldsymbol{e}}_p^{\omega_\alpha}$ exist in all ω_α of the mesh, it can be shown that

$$\|\boldsymbol{e}_p\|_E^2 = \mathscr{B}(\boldsymbol{e}_p,\boldsymbol{e}_p) = \sum_{\alpha=1}^{N} \mathscr{R}\left(\varphi_\alpha \boldsymbol{e}_p\right) \tag{35}$$

using Eqs. (8) and (20). The error field $\boldsymbol{e}_p$ of an approximation of degree $\boldsymbol{u}_p$, being a continuous functions from an infinite functions space $\mathcal{V}$ as Eq. (5), provides an upper bound in terms of the energy norm of the exact error field (Prudhomme et al. , 2004; Mariné, 2005; Parés, Díez & Huerta, 2006; Strouboulis et al., 2006).

Therefore, following Strouboulis et al. (2006)

$$\|\boldsymbol{e}_p\|_E^2 \leq \sqrt{\sum_{\alpha=1}^{N} \|\boldsymbol{e}_p^{\omega_\alpha}\|_{E(\omega_\alpha)}^2}\, \sqrt{M\mathscr{B}(\boldsymbol{e}_p,\boldsymbol{e}_p)} = \sqrt{\sum_{\alpha=1}^{N} \|\boldsymbol{e}_p^{\omega_\alpha}\|_{E(\omega_\alpha)}^2}\, \sqrt{M}\, \|\boldsymbol{e}_p\|_E \tag{36}$$

and a global estimate $\mathcal{E} = \|\boldsymbol{e}_p\|$ is now defined in terms of the approximated error field $\tilde{\boldsymbol{e}}_p^{\omega_\alpha}$ as

$$\mathcal{E} = \sqrt{M}\sqrt{\sum_{\alpha=1}^{N} \left\|\tilde{\boldsymbol{e}}_p^{\omega_\alpha}\right\|_{E(\omega_\alpha)}^2}\,, \quad \text{with} \quad \|\tilde{\boldsymbol{e}}_p^{\omega_\alpha}\|_{E(\omega_\alpha)}^2 = \mathscr{B}_{\omega_\alpha}^{\zeta_\alpha}\left(\tilde{\boldsymbol{e}}_p^{\omega_\alpha},\tilde{\boldsymbol{e}}_p^{\omega_\alpha}\right) \tag{37}$$

where M is the overlapping index of the employed partition of unity, that comes from the choice $\zeta_\alpha = 1$ in Eq. (23) (Strouboulis et al., 2006). In case $\zeta_\alpha = \varphi_\alpha$, according to Prudhomme et al. (2004), a global estimate $\mathcal{E}^{\varphi_\alpha} = \|\boldsymbol{e}_p\|$ is computed as

$$\mathcal{E}^{\varphi_\alpha} = \sqrt{\sum_{\alpha=1}^{N} \left\| \tilde{e}_p^{\omega_\alpha} \right\|^2_{E(\omega_\alpha)}} \tag{38}$$

in such a way the weighting of the energy from the error allows to verify the condition expressed in Eq. (27), and therefore avoiding the superposition evidenced by the overlapping index M in Eq. (37).

Additionally, the nodal error indicators are computed as

$$\mathcal{I}_{\omega_\alpha} = \sqrt{M \left\| \tilde{e}_p^{\omega_\alpha} \right\|^2_{E(\omega_\alpha)}} \quad \text{and} \quad \mathcal{I}_{\omega_\alpha}^{\varphi_\alpha} = \sqrt{\left\| \tilde{e}_p^{\omega_\alpha} \right\|^2_{E(\omega_\alpha)}} \tag{39}$$

considering $\zeta_\alpha = 1$ and $\zeta_\alpha = \varphi_\alpha$, respectively (Strouboulis et al., 2006; Prudhomme et al., 2004).

5 NUMERICAL EXAMPLE

The classical problem of a L-shaped domain, loaded by tractions given by the analytical solution for stresses, according to Szabó & Babuška (2011), is analyzed, considering plane strain state. For the computation of such tractions the following values were considered: $a_1 = 1.0$, $\lambda_1 = 0.544\,483\,737$ and $Q_1 = 0.543\,075\,579$. Moreover, for the results reported here, the characteristic dimension for such L-shaped domain (the length of the two sides that share the reentrant corner) is $a = 100.0$, and the thickness is $l_z = 1.0$, both having units of length, $[L]$.

The material properties considered are the Young modules $E = 1000$, with units $[F]/[L]^2$, with [F] being the unit of force, and Poisson ratio $\nu = 0.3$. The exact energy norm is provided by Barros, Proença & Barcellos (2004), considering the exact solution provided by Szabó & Babuška (2011).

Four different meshes are used (Fig. 1), for which the approximations $\boldsymbol{u}_p$ are computed considering $p = 1$. The rigid body motions are suppressed by applying the pointwise restrictions $u_x(0,0) = u_y(0,0) = u_y(141.42,0) = 0$.

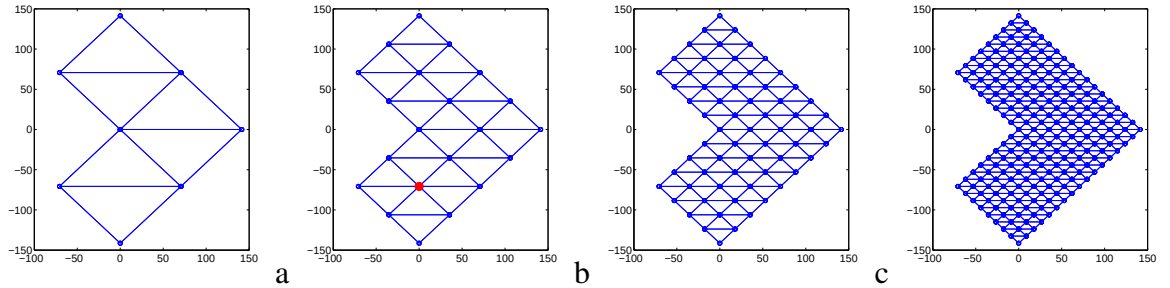

Figure 1: Four different nested meshes, in which there are only convex clouds. Therefore, since exponential edge functions are used, the approximated solutions herein have continuity $C^\infty(\Omega)$.

The local problems for the error on the cloud are computed using Eq. (29). For the bilinear form $\mathscr{B}^{\zeta_\alpha}_{\omega_\alpha}$, the both cases, $\zeta_\alpha = 1$ and $\zeta_\alpha = \varphi_\alpha$ are considered, following Strouboulis et al. (2006) and Prudhomme et al. (2004), respectively. Therefore, the nodal error indicators are computed using Eq. (39) and the global estimators are computed using Eqs. (37) and (38).

Herein, the estimations are performed only using $q = 1$, in other words, only considering one polynomial degree higher than the approximated solution. Thus, the estimated error energy is computed from functions in Eq. (28) with $p+q = 2$.

Figure 2 shows the cartesian components of the strong-form residuum field, computed using Eq. (32), associated with the approximation $\boldsymbol{u}_p$ with degree $p = 1$ for the mesh in Figure 1b. Such field is a vector valued function as the displacement field, and it has dimensions $[F]/[L]^3$, similar to the body force $\boldsymbol{b}$ (see Section 2), disregarded herein.

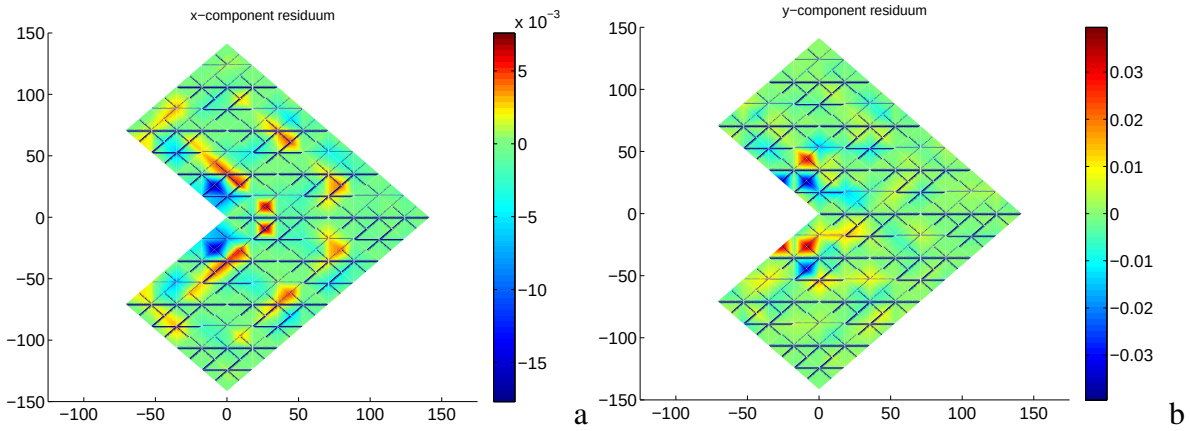

Figure 2: Strong-form residuum field for the approximation u_p, with $p = 1$, using the second mesh (from left to right) in Figure 1. (a) x-component. (b) y-component.

Is is worth to note that the C^k-GFEM methodology allows to compute continuous residuum field directly, without any type of smoothing operation in the post-processing stage. The magnitudes showed in the color scales mean the error in the internal force per volume unit, for each cartesian direction. In case the approximation $\boldsymbol{u}_p$ reaches the exact solution of the problem, the residuum field is null on the entire domain, meaning that the strong form equilibrium equations are satisfied everywhere. Therefore, it should be noted that such residuum field is not an error field $\boldsymbol{e}_p$, but can be understood as a body force associated to it.

For these results, the Wandzura symmetric triangle integration rule (Wandzura & Xiao, 2003), with 175 points, was used for all integrations over element domains, for composing the global stiffness matrices or to build the local stiffness matrices for error estimation. Additionally, the Gauss-Legendre rule with 25 points was used for all numerical integrations on element edges.

As the procedure presented herein involves the strong-form residuum of the Neumann boundary conditions in Eq. (33), it should be noted that contributions from the error in the natural boundary conditions, for the local error problems of Eq. (29), raise along the entire boundary $\partial\Omega$. Figure 3a shows the non-null externally applied tractions $\bar{\boldsymbol{t}}$ for composing Eq. (7) (see Section 2), whereas Fig. 3b shows the computed error in the natural boundary condi-

tions, for the same mesh as in Fig. 2, considering approximation with degree $p = 1$. Note that there is such residuum even along the reentrant edges, where homogeneous Neumann boundary conditions were prescribed, and it means the error in the normal derivative of the approximation.

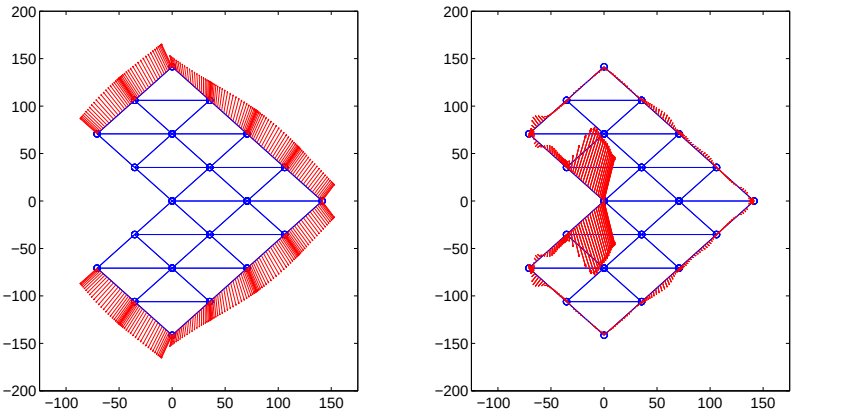

Figure 3: Tractions along the domain boundary. (a) Non-null externally applied surface forces. (b) Strong-form residuum along the boundary.

Figure 4 shows the x-component of the local approximated error field $\tilde{e}_p^{\omega_\alpha}$, solution of Eq. (29), for the cloud associated with the node marked in red color in Fig. 1b, for the two tested ways of weighting the bilinear form in Eq. (23). It may be seen that the error field is null right on the seven nodes covered by such cloud, in accordance with the feature commented in the **Remark 5**.

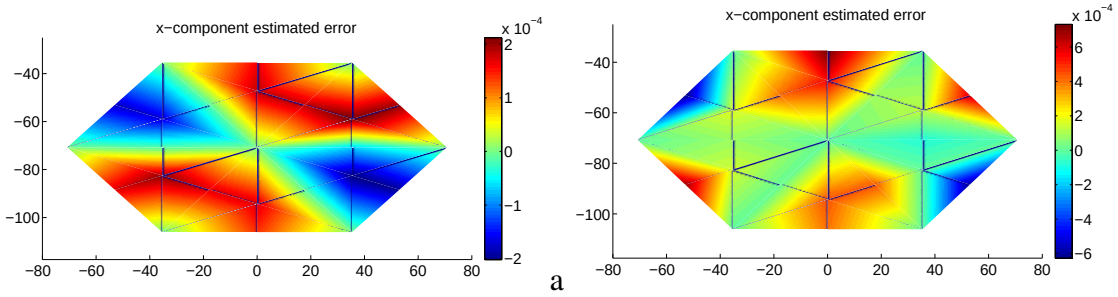

Figure 4: x-component of the local estimated error field $\tilde{e}_p^{\omega_\alpha}$, with $p = 1$ and $q = 1$, on the cloud ω_α associated to the node in red color in Fig. 1b. (a) Considering $\zeta_\alpha = 1$ (Strouboulis et al., 2006). (b) Considering $\zeta_\alpha = \varphi_\alpha$ (Prudhomme et al., 2004).

The nodal effectivity indices are displayed in Fig. 5. It may be seen that a slightly local overestimation right at the reentrant corner ensures the identification of the critical point. Some overestimations on boundary nodes also happen for this coarse mesh (Fig. 1b), probably due the low degree of the approximation.

Finally, the global effectivity indices are displayed in Fig. 6. Such index is defined as a ratio between the estimated error and the exact one, a measure that is possible for this model

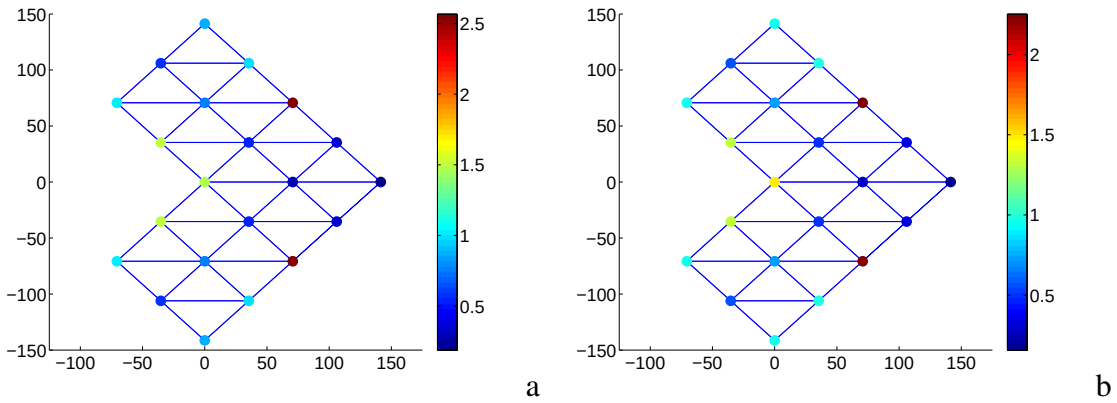

Figure 5: Local effectivity, the ratio between the nodal indicator and the exact error associated to the node. (a) Considering $\mathcal{I}_{\omega_\alpha}$, when $\zeta_\alpha = 1$ in Eq. (23), following Strouboulis et al. (2006). (b) $\mathcal{I}_{\omega_\alpha}^{\varphi_\alpha}$, when $\zeta_\alpha = \varphi_\alpha$ in Eq. (23), following Prudhomme et al. (2004).

problem because the exact solution is known. The global estimators are computed by Eqs. (37) and (38). For the curves, each point is related to a mesh of Fig. 1, considering approximations of degree $p = 1$ and using functions of one degree higher for error estimation.

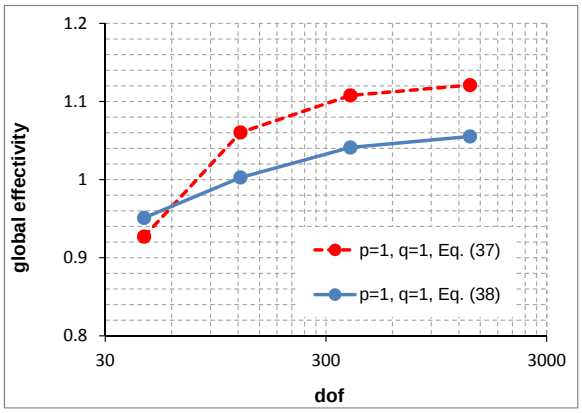

Figure 6: Global effectivity, the ratio between the estimator and the exact global error, considering $\mathcal{E}$ defined in Eq. (37), when $\zeta_\alpha = 1$ in Eq. (23), following Strouboulis et al. (2006), and $\mathcal{E}^{\varphi_\alpha}$ defined in Eq. (38), when $\zeta_\alpha = \varphi_\alpha$ in Eq. (23), following Prudhomme et al. (2004).

6 CONCLUDING REMARKS

The proposed way of computing the residual functional for cloud-based error estimators exploits the continuity provided by continuous approximation functions generated through the C^k–GFEM. Additionally, it allows to benefit from some information from higher-order derivatives of the approximations.

An investigation on the effects on the integration cost is being carried out. Results for the global effectivity, considering different degrees of approximations will be presented in a forthcoming paper.

Additionally, an improvement which is a direct extension of this subdomain procedure is to consider a localization of the residual functional in Eq. (20) using a step function ψ_α such that $\psi_\alpha = 1$ on the cloud and equal to zero outside the cloud. Firstly, it should be remembered that the original goal of performing the localization in Eq. (20) using the PoU φ_α is to avoid equilibrating procedures required in conventional element-based estimators and the line integration of Neumann boundary conditions along the cloud boundary (see **Remark 3** and **Remark 4**). When using smooth approximation functions, both the stress and residuum fields are continuous and, therefore, the residuum along the cloud boundaries ω_α may provide Neumann boundary conditions for the problems on the clouds. This approach will be investigated.

ACKNOWLEDGEMENTS

D. A. F. Torres gratefully acknowledge the financial support for payment the congress registration fee provided by UTFPR at Londrina, through the DIRPPG 03/2016 Official Notice. C. S. de Barcellos and F. B. Barros gratefully acknowledge the financial support provided by the Brazilian government agency CNPq (Conselho Nacional de Desenvolvimento Científico e Tecnológico) under the research grants 304.698/2013-0 (Barcellos), 309.005/2013-2 and 486.959/2013-9 (Barros).

REFERENCES

Ainsworth, M., & Oden, J. T., 2000. *A posteriori error estimation in finite element analysis*. John Wiley and Sons.

Anuvriev, I., Korneev, V., & Kostylev, V., 2007. *A posteriori error estimation by means of the exactly equilibrated fields*. Austrian Academy of Sciences, Institutional Report.

Babuška, I., & Strouboulis, T., 2001. *The finite element method and its reliability*. Oxford.

Babuška, I., Whiteman, J. R., & Strouboulis, T., 2011. *Finite elements: an introduction to the method and error estimation*. Oxford.

Barcellos, C. S. de, Mendonça, P. T. R., & Duarte, C. A., 2009. A C^k continuous generalized finite element formulation applied to laminated Kirchhoff plate model. *Computational Mechanics*, vol. 44, pp. 377–393.

Barros, F. B., Barcellos, C. S. de, & Duarte, C. A., 2007. p-Adaptive C^k generalized finite element method for arbitrary polygonal clouds. *Computational Mechanics*, vol. 41, pp. 175–187.

Barros, F. B., Barcellos, C. S. de, & Duarte, C. A., 2009. Subdomain-based flux-free a posteriori estimator for generalized finite element method. *Thirth Ibero-Latin-American Congress on Computational Methods in Engineering (XXX-CILAMCE)*

Barros, F. B., Barcellos, C. S. de, Duarte, C. A., & Torres, D. A. F., 2013. Subdomain-based error techniques for generalized finite element approximations of problems with singular stress fields. *Computational Mechanics*, vol. 52, pp. 1395–1415.

Barros, F. B., Proença, S. P. B., & Barcellos, C. S. de, 2004. On error estimator and p-adaptivity in the generalized finite element method. *International Journal for Numerical Methods in Engineering*, vol. 60, pp. 2373–2398.

Belytschko, T., & Black, T., 1999. Elastic crack growth in finite elements with minimal remeshing. *International Journal for Numerical Methods in Engineering*, vol. 45, pp. 601–620.

Belytschko, T., & Gracie, R., 2007. On XFEM applications to dislocations and interfaces. *International Journal of Plasticity*, vol. 23, n. 10, pp. 1721–1738.

Boresi, A. P., Chong, K. P., & Lee, J. D., 2011. *Elasticity in engineering mechanics*. 3rd. ed., John Wiley and Sons.

Brebbia, C. A., Telles, J. C. F., & Wrobel, L. C., 1984. *Boundary element techniques: theory and applications in engineering*. Springer-Verlag.

Díez, P., Parés, N., & Huerta, A., 2004. Accurate upper and lower bounds by solving flux-free local problems in stars. *Revue Européenne des Eléments Finis*, vol. 13, pp. 497–507

Duarte, C. A., 1996. *The hp-cloud method*. PhD thesis, The University of Texas at Austin.

Duarte, C. A., Babuška, I., & Oden, J. T., 2000. Generalized finite element method for three-dimensional structural mechanics problems. *Computers and Structures*, vol. 77, pp. 215–232.

Duarte, C. A., Kim, D. J., & Quaresma, D. M., 2006. Arbitrarily smooth generalized finite element approximations. *Computer Methods in Applied Mechanics and Structures*, vol. 196, pp. 33–56.

Duarte, C. A., & Oden, J. T., 1996. An $h-p$ adaptive method using cloud. *Computer Methods in Applied Mechanics and Engineering*, vol. 139, pp. 237–262.

Freitas, A., Torres, D. A. F., Mendonça, P. T. R., & Barcellos, C. S. de, 2015. Comparative analysis of C^k- and C^0-GFEM applied to two-dimensional problems of confined plasticity. *Latin American Journal of Solids and Structures*, vol. 12, n. 5, pp. 861–882.

Fries, T. P., & Belytschko, T., 2010. The extended/generalized finite element method: an overview of the method and its applications. *International Journal for Numerical Methods in Engineering*, vol. 84, pp. 253–304.

Kreyszig, E., 1989. *Introductory Functional Analysis with Applications*. Wiley.

Ladevèze, P., & Leguillon, D., 1983. Error estimate procedure in the finite element method and applications. *SIAM Journal on Numerical Analysis*, vol. 20, pp. 485–509.

Liu, G. R., 2003. *Mesh free methods: moving beyond the finite element method*. CRC Press.

Mariné, N. P., 2005. *Error assessment for functional outputs of PDE's: bounds and goal-oriented adaptivity*. PhD thesis, Universitat Politècnica de Catalunya.

Mendonça, P. T. R., Barcellos, C. S. de, & Torres, D. A. F., 2011. Analysis of anisotropic Mindlin plate model by continuous and non-continuous GFEM. *Finite Elements in Analysis and Design*, vol. 47, pp. 698–717.

Mendonça, P. T. R., Barcellos, C. S. de, & Torres, D. A. F., 2013. Robust C^k/C^0 generalized FEM approximations for higher-order conformity requirements: application to Reddy's HSDT model for anisotropic laminated plates. *Composite Structures*, vol. 96, pp. 332–345.

Morin, P., Nochetto, R. H., & Siebert, K. G., 2003. Local problems on stars: a posteriori error estimators, convergence, and performance. *Mathematics of Computations*, vol. 72, pp.

1067–1097.

Oden, J. T., Demkowicz, L., Rachowicz, W., & Westermann, T. A., 1989. Toward a universal $h-p$ adaptive finite element strategy. Part 2: A posteriori error estimation. *Computer Methods in Applied Mechanics and Engineering*, vol. 77, pp. 113–180.

Oden, J. T., Duarte, C. A., & Zienkiewicz, O. C., 1998. A new cloud-based *hp* finite element method. *Computer Methods in Applied Mechanics and Engineering*, vol. 153, pp. 117–126.

Oden, J. T., & Reddy, J. N., 1976. *An introduction to the mathematical theory of finite elements*. Wiley.

Parés, N., Díez, P., & Huerta, A., 2006. Subdomain-based flux-free a posteriori error estimators. *Computer Methods in Applied Mechanics and Engineering*, vol. 195, pp. 297–323.

Prudhomme, S., Nobile, F., Chamoin, L., & Oden, J. T., 2004. Analysis of a subdomain-based error estimator for finite element approximations of elliptic problems. *Numerical Methods for Partial Differential Equations*, vol. 20, pp. 165–192.

Rvachev, V. L., & Sheiko, T. I., 1995. *R*-functions in boundary value problems in mechanics. *Applied Mechanics Reviews*, vol. 48, pp. 151–188.

Shepard, D., 1968. A two-dimensional interpolation function for irregularly-spaced data. 23rd ACM National Conference, pp. 517–524.

Simone, A., Duarte, C. A., & Giessen, E. V. der, 2006. A generalized finite element method for polycrystals with discontinuous grain boundaries. *International Journal for Numerical Methods in Engineering*, vol. 67, pp. 1122–1145.

Stazi, F. L., Budyn, E., Chessa, J., & Belytschko, T., 2003. An extended finite element method with higher-order elements for curved cracks. *Computational Mechanics*, vol. 31, pp. 38–48.

Strouboulis, T., Babuška, I., & Copps, K., 2000. The design and analysis of the generalized finite element method. *Computer Methods in Applied Mechanics and Engineering*, vol. 181, pp. 43–69.

Strouboulis, T., Copps, K., & Babuška, I., 2001. The generalized finite element method. *Computer Methods in Applied Mechanics and Engineering*, vol. 190, pp. 4081–4193.

Strouboulis, T., Zhang, L., & Babuška, I., 2003. Generalized finite element method using mesh-based handbooks: application to problems in domains with many voids. *Computer Methods in Applied Mechanics and Engineering*, vol. 192, pp. 3109–3161.

Strouboulis, T., Zhang, L., Wang, D., & Babuška, I., 2006. A posteriori error estimation for generalized finite element methods. *Computer Methods in Applied Mechanics and Engineering*, vol. 195, pp. 852–879.

Szabó, B., & Babuška, I., 2011. *Introduction to finite element analysis: formulation, verification and validation*. Wiley.

Torres, D. A. F., 2012. *Contributions on the use of continuous approximation functions in the generalized finite element method: evaluation in fracture mechanics*. PhD thesis (in portuguese), Federal University of Santa Catarina.

Torres, D. A. F., Barcellos, C. S. de, & Mendonça, P. T. R., 2015. Effects of the smoothness of partitions of unity on the quality of representation of singular enrichments for GFEM/XFEM stress approximations around brittle cracks. *Computer Methods in Applied Mechanics and Engineering*, vol. 283, pp. 243–279.

Torres, D. A. F., Mendonça, P. T. R., & Barcellos, C. S. de, 2011. Evaluation and verification of an HSDT-layerwise generalized finite element formulation for adaptive piezoelectric laminated plates. *Computer Methods in Applied Mechanics and Engineering*, vol. 200, pp. 675–691.

Wandzura, S., & Xiao, H., 2003. Symmetric quadrature rules on a triangle. *Computers and Mathematics with Applications*, vol. 45, pp. 1829–1840.